Chinese Chemical Letters 31 (2020) 2119–2124

Contents lists available at ScienceDirect

Chinese Chemical Letters

journal homepage: www.elsevier.com/locate/cclet

Communication

Novel, tadpole-shaped, polyhedral oligomeric silsesquioxane containing sulfonated block copolymer for humidity sensing

Fang Chen*, Jiayu Yang, Rong Cai, Mengfei Qi, Xiaoyan Ma*

The Key Laboratory of Polymer Science and Technology of Shaanxi Province, School of Chemistry and Chemical Engineering, Northwestern Polytechnical University, Xi'an 710129, China

ARTICLE INFO

Article history:
Received 14 October 2019
Received in revised form 1 January 2020
Accepted 2 January 2020
Available online 21 January 2020

Keywords:
POSS containing block copolymer
Tadpole-shaped
Humidity sensor
Sulfonation degree
Wide impedance response

ABSTRACT

Due to the "trade-off" effect between the high water adsorption and low stability under high Relative Humidity of polymer matrix, fabrication of resistive-type polymer-based humidity sensors with a wide impedance response and excellent stability in high relative humidity remains a great challenge. Aim at solving that, a novel polymeric humidity sensing matrix, specifically a tadpole-shaped, polyhedral oligomeric silsesquioxane (POSS) containing block copolymers (BCPs) of POSS-poly(methyl methacrylate)-polystyrene (POSS-PMMA-SPS) were proposed. This novel BCP was synthesized using atom transfer radical polymerization (ATRP) employing a two-step approach, and following post sulfonation, a series of sulfonated BCPs (POSS-PMMA-SPS) with different sulfonation degree was obtained. The subject humidity sensors were produced using different sulfonated BCPs employing a dip-coating technique, and three wide-impedance response humidity sensors were produced. Each of these sensors exhibited an excellent humidity-sensing response of more than 10^4 within the humidity range from 11% to 95% RH. In particular, the humidity sensor S-6 that had a proper degree of sulfonation presented a relatively fast response ($t_{90\%}$ of 11 s and 80 s in both the water adsorption and desorption processes), and superior repeatability for more than 30 days.

Accurate humidity detection is very important in many industries, including food production, plant cultivation, medical care, drug manufacturing, *etc*. Up to now, fabricating the humidity sensor with excellent sensing response [1], lower cost [2], fast respond [3] and multifunctional applications [4] is highly demanded. During the past several decades, various types of humidity sensitive materials have been closely investigated including, inorganic ceramics [5–8], polymer [9–11], carbon based materials [12], organic-inorganic composites [13–15] and novel low dimensional materials [16]. Among these popular materials, polymer-based sensing materials have received the most attention due to their tunable molecular structure as well as the excellent humidity sensing property, *etc.*

The polyelectrolyte was the first generation of polymer resistive-type humidity sensing materials that exhibited very low stability in high relative humidity (RH) due to the high solubility of the polymer. Many techniques designed to reduce the solubility of polyelectrolytes in high RH have been investigated including intermolecular cross-linking [10,17,18] and interpenetrating polymer networks [19] and these have been proven to be effective in reducing this problem. However, low sensitivity in low RH has been identified as the second technical barrier for polymer based resistive-type sensor materials. To address this condition, various kinds of polymer composites (primarily polyelectrolytes) combined with highly conductive materials, such as carbon black, carbon nanotubes, graphene, and intrinsic conductive polymers have been investigated [20].

Based on previous research, some improvements in the sensing response of polymer resistive-type humidity sensing materials have been achieved. However, the trade-off effect between high water adsorption and low stability under high RH of the polymer sensing matrix is still hard to solve. Previous studies on ion-containing block copolymers (BCP), have shown that this type of materials is a promising polymer matrix for ion exchange membranes, proton exchange membrane fuel cell(PEMFC) [21–23] and humidity sensors [24] due to their promising properties in terms of well determined molecular structure, self-assembly behavior [25] and tunable morphology resulting from micro-phase separation [26].

Zhang [27] described the synthesis of a cross-linked organic-inorganic framework based on polyhedral oligomeric

* Corresponding authors.
E-mail addresses: chenfang820811@nwpu.edu.cn (F. Chen), m_xiao_yana@nwpu.edu.cn (X. Ma).

https://doi.org/10.1016/j.cclet.2020.01.020
1001-8417/

silsesquioxane (POSS), which exhibited a fast humidity response and recovery time. However, the impedance response range of this material was limited to three orders of magnitude. In addition, ionic POSS containing BCPs [28] have been reported as a promising PEM candidate to solve the trade-off effect between mechanical strength and proton conductivity under low RH.

Therefore, in this present study, we report on the synthesis of a novel tadpole-shaped ion containing POSS based BCP that exhibited both a wide impedance response and excellent stability in high RH. The POSS core provides structural rigidity due to chemical bonding to the polymer matrix, and the hydrophilic sulfonated polystyrene provides high capacity for water adsorption and desorption. By precisely manipulating the synthesis conditions *via* atom transfer radical polymerization (ATRP), a well-defined structure of the POSS BCP was achieved. After comparing the humidity sensing properties of the POSS BCP with different degrees of sulfonation, it was determined that the POSS BCP with a proper sulfonation degree exhibited excellent humidity sensing performance.

In this study, POSS-PMMA-PS was polymerized using a two-step ATRP route as shown in Scheme S1 (Supporting information), which produced a BCP with polydispersity of M_w/M_n = 1.76 and M_n = 72300 which is determined by gel permeation chromatograph GPC. After the synthesis of BCP, post-sulfonation was accomplished using concentrated sulfuric acid as the sulfonation agent, the chemical structure of sulfonated BCP is presented in Scheme 1.

The FT-IR spectra are shown in Figs. 1a and b, the absorbance band around 1172 cm^{-1} is attributed to the asymmetrical stretching vibration of the S=O group. Two absorption peaks at 1034 cm^{-1} (S—O, symmetric stretching) and 1006 cm^{-1} (CH—, in-plane bending of para disubstituted phenyl ring) are observed. These main peaks show that sulfonated pendant moieties are successfully grafted onto the PS chain. Moreover, there are great differences in two characteristic peaks at 699 and 759 cm^{-1}, which are attributed to the out-of-plane skeleton bending vibrations of the benzene ring and the out-of-plane bending vibration of the five —CH— groups in the monosubstituted benzene ring [29]. The ^{1}H NMR spectrum of POSS-PMMA-PS shown in Fig. 1c. As presented, two tiny bands from 1.01 and 0.83 ppm correspond to the protons (H_d) in the methyl group. At the same time, the appearance of methoxy protons (—OCH_3) shows as a sharp peak at 3.79 ppm (H_e), which is an indication of the successful synthesis of POSS-PMMA. After the completion of the ATRP synthesis in the second step, two tiny sharp peaks at 1.88 and 1.91 ppm are found in the spectrum that are attributed to the methylene protons (—CH_2-, H_f and H_g), and the proton resonances of the benzene protons were observed at 6.44 and 7.25 ppm (H_a, H_h). This is an indication of the successful synthesis of POSS-PMMA-PS. ^{1}H NMR spectra of the POSS-PMMA-SPS is shown in Fig. 1d. In Fig. 1d, a clear peak at 7.52 ppm is observed and assigned to the aromatic proton next to the SO_3^{2-}group (H_c) after sulfonation, and the peaks at 7.1 ppm (H_b) and 6.6 ppm ($H_{a,a'}$) are attributed to other aromatic protons on both the sulfonated and unsulfonated phenyl rings. It could prove the introduction of sulfonic acid groups to phenyl groups. Combined with the FTIR and ^{1}H NMR analysis, it is concluded that the BCP was indeed synthesized and successfully sulfonated.

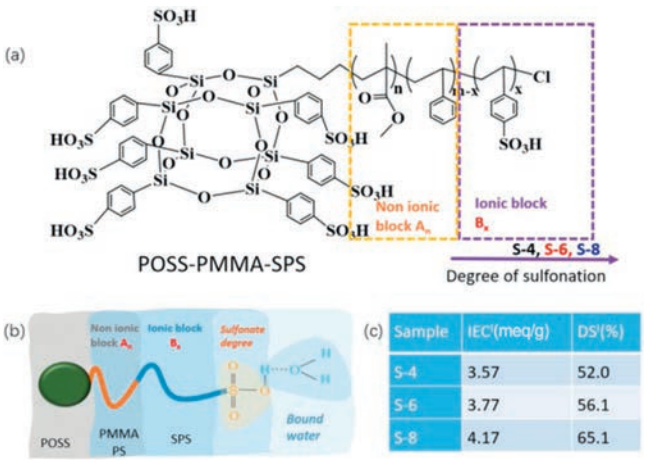

Sample	IEC[1](meq/g)	DS[1](%)
S-4	3.57	52.0
S-6	3.77	56.1
S-8	4.17	65.1

Scheme 1. Chemical structure and physical property of POSS-PMMA-SPS with different sulfonation degree (S-4, S-6 and S-8). (a) Chemical structure; (b) schematic illustration of POSS-PMMA-SPS; (c) ion exchange capacity(IEC) and degree of sulfonation (DS) of different BCP. I: The IEC and DS value was calculated through titration as indicated in Supporting information.

The mechanism of the response of the resistive-type polymer humidity sensor is based on the variation of its impedance under different RH. The polymer-water interaction of the polymer sensing materials is the key issue in the performance of the humidity sensor, which is linked to the variation in its physical or chemical water adsorption behavior. Polyelectrolytes produce changes in their resistivity in response to variations in RH, which is mainly attributed to the dependence of the polymer's ionic impedance on changes in the ionic strength due to changes in RH. In general, an ionic polymer matrix is composed of hydrophobic and hydrophilic domains. The hydrophilic segments are represented by the sulfonated acid moieties that enable the ionic polymer to adsorb water. In this reported study, S-4, S-6 and S-8 are produced with different ion exchange capacity (IEC), which shows them to be 3.57, 3.77 and 4.17 meq/g, respectively as shown in Scheme 1c. In Fig. 2a, it can be seen that the water uptake of these various materials increased with the increase in RH as a result of the variation in the IEC values. S-8 appears to have the highest water uptake over the whole RH range due to the higher concentration of sulfonated moieties within the polymer matrix. Hence, the λ values can be calculated from the water uptake value in different RH, which represents the number of water molecules per sulfonic group in the ionic block copolymer. The hydration number of the sulfonated BCPs with different degrees of sulfonation versus RH is plotted in Fig. 2b. In accordance with the trend of increasing of water uptake as the RH increased, λ exhibited a similar increase that coincided with the increase in the IEC. In addition, a rationale for the water adsorption behavior of ionic BCP was developed as shown in Fig. S1 (Supporting information).

As indicated in experimental section, humidity sensors comprised of variations of sulfonated BCPs with different IEC values were obtained by dip coating the polymer solutions onto blank ceramic interdigitated electrodes. Then the humidity response of the treated electrodes was determined by measuring the variation in the sensor's impedance in different RH environments. To begin with, we carried out the relative impedance at various frequencies in different RHs to determine the best working frequency for the humidity sensor for a series of sulfonated BCPs (Fig. S2 in Supporting information). At frequency of 100 Hz, all three samples exhibited good linear impedance behavior as a function of relative humidity, showing that this may be a useful means for measuring RH using these sensors under this frequency. Fig. 3 summarizes the RH test results for these sensors showing that they respond linearly to the various levels of RH. As shown, the impedance signals of the three sensors significantly decrease with the increase in RH over the whole RH range and the difference in the impedance values is four orders of magnitude from a RH at 11%–95%. In fact, the impedance of sulfonated polymers at different RH are influenced by two factors, the density of sulfonated groups and dissociation coefficient of protons from sulfonated groups [30]. According to our analysis, S-4, S-6 and S-8 are produced with different IEC values, which shows them to be

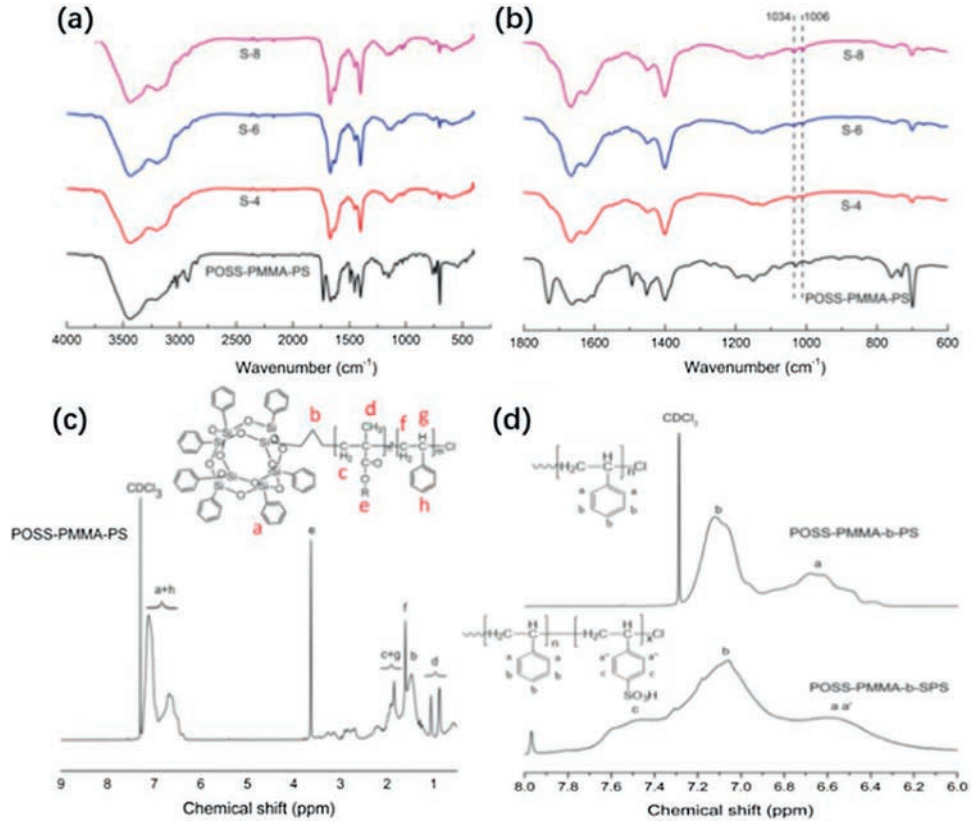

Fig. 1. Structural characterization of POSS-PMMA-PS and POSS-PMMA-SPS. Comparison of FT-IR spectra based on POSS containing BCPs (a) wavenumber from 4000 cm^{-1} to 250 cm^{-1}, (b) wavenumber from 1800 cm^{-1} to 600 cm^{-1}. ^1H NMR spectra of (c) POSS-PMMA-PS and (d) POSS-PMMA-SPS.

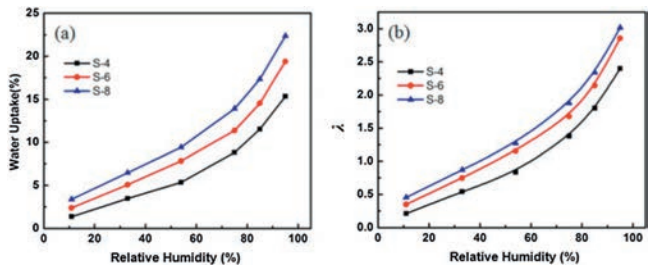

Fig. 2. The water adsorption of POSS-PMMA-SPS with different sulfonation time as the function of RH (a). The effect of RH on hydration number (λ) at 30 °C for POSS-PMMA-SPS with different sulfonation time (b).

3.57, 3.77 and 4.17 meq/g, respectively. However, the number of water molecular per sulfonated group is relative low (all less than 3), which means the dissociation of protons from sulfonated groups are highly suppressed since the adsorbed water molecules are very limited. Therefore, the higher sulfonated group density (S-8), the higher suppression of dissociation, lead to decreasing of impedance at high RH than the other two copolymers. This illustrated that all three sensors exhibit a relative wide humidity sensing range compared to previously reported polymer resistive-type humidity sensing materials [24].

In addition to the humidity response, the hysteresis behavior upon exposure to humid air is a very important parameter used to evaluate the performance of a humidity sensor. The humidity hysteresis behavior of three sensors in the RH range from 11% to 95% is shown in Fig. S3 (Supporting information), and the humidity hysteresis is listed in Table 1.

The S-6 sensor exhibited the least humidity hysteresis of the three sensors. Based on previous arguments about water adsorption behavior in Supporting information, the humidity hysteresis behavior is related to the interaction between the water and the polymeric matrix, and is attributed primarily to the hydrophilic clusters. In the case of the POSS BCPs, when the results for sample S-8 are compared to those for S-6, it appeared that S-6 may aggregate to form smaller domains of hydrophilic clusters when water is adsorbed. This would facilitate fast water desorption at lower RH. Maintaining a balance between the water adsorption and water interaction with the polymer matrix is the crucial issue in the fabrication of low humidity hysteresis polymer-based humidity sensors.

The third requirement of a good humidity sensor is a fast response and recovery time. As has been reported in previous publications, a slow recovery time was found to be a universal technical barrier for practical application of polymer-based humidity sensor. The desired response time of adsorption and recovery from desorption has been determined to be the achievement of 90% of the full impedance change when humidity changes from 11% to 95% and *vice versa*. As shown in Fig. 4a, the response time of the sensors was 15 s for S-4, 11 s for S-6, and 12 s for S-8. From the data shown in Fig. 4b, it can be seen that the recovery time for the various sensors was 88 s for S-4, 80 s for S-6 and 100 s for S-8. Table 1 lists the sensing performance of the POSS-PMMA-SPS based humidity sensors and compares these results with reported literature values. These data show that the POSS-PMMA-SPS is a very promising material for use in humidity sensors since it provides relative low hysteresis and short response and recovery times.

Long-term stability is another metric that must be met for the commercial humidity sensor applications. Since the exposure environment for humidity detection is complex, a fluctuating impedance at low and high humidity during the cycling will

Table 1
Comparison of sensing performance of POSS-PMMA-PS and other reported polymer based sensing materials.

Sensing material	Detection range (RH)	Impedance variation (Ω)	Hysteresis (RH)	Response time (s)	Recovery time (s)	References
S-4	11%–95%	1.9×10^6–3.2×10^2	>10% RH	15	88	this work
S-6	11%–95%	1.7×10^6–8.7×10^1	6% RH	11	80	this work
S-8	11%–95%	1.9×10^6–5.4×10^2	9% RH	12	100	this work
MPOSS	33%–95%	1×10^7–5×10^3	1.5% RH	3	40 ± 4	[26]
Sulfonated polyimides	30%–90%	1×10^4–5×10^1	6% RH	60	240	[31]
PDEAEMA-*b*-PS	22%–95%	8.98×10^8–2.97×10^4	8% RH	60	206	[24]

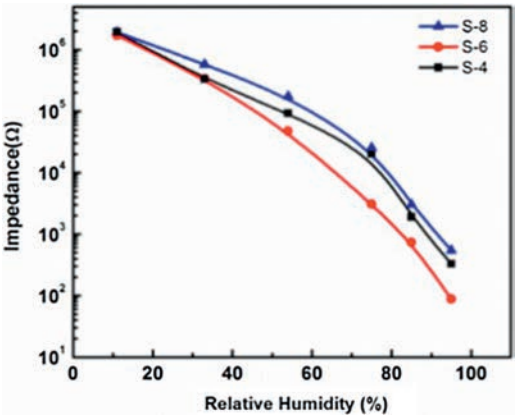

Fig. 3. Humidity responsive curve of POSS-PMMA-SPS with different sulfonation time.

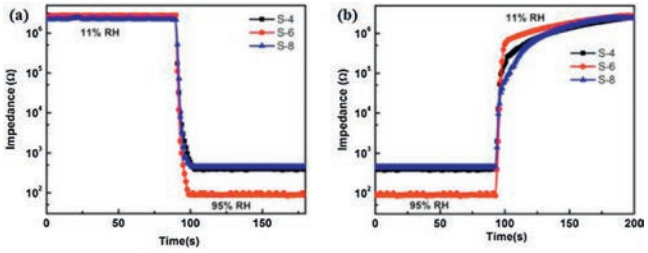

Fig. 4. The response properties (a) and the recovery properties (b) of POSS-PMMA-SPS humidity sensors.

disqualify a sensor for use. The sensing performance of humidity sensors might significantly deteriorate after long term exposure, particularly when exposed to low and high RH. To evaluate the performance stability of the material, all three humidity sensors were exposed to 11% RH and 95% RH for 30 days and the impedance fluctuation of three humidity sensors is shown in Figs. 5a–c. In order to illustrate the stability of the humidity sensors, the fluctuation values (ΔZ) with time is given by $\Delta Z = (\log Z_n - \log Z_0)/\log Z_0 \times 100\%$, where $\log Z_n$, $\log Z_0$ denote the impedance of each humidity sensor on the n and 0 day, respectively. Fig. 5d summarize the maximum and average fluctuation value of three humidity sensors. Taking S-6 humidity sensor for example, the calculation results show that the maximal fluctuation value is -5.4% on 30th days at 95% RH, and the average fluctuation values of 11%, 33%, 54%, 75%, 85%, 95% RH in a month are 0.1%, 0.4%, -2.6%, 0.5%, 0.7% and -1.9%, respectively. The slight fluctuation of impedance proves excellent stability and durability of S-6 humidity sensor.

The complex impedance plots under different RH can be represented by the equivalent circuits with the resistor, the capacitor and Warburg impedance in series and parallel (R_f: resistor; C_f: capacitor, Z_w: Warburg impedance). In Fig. 6, while the RH is relative low (11%–54% RH), the impedance plots could be represented by an arc at 11% RH and the semicircles at 33% and 54% RH, respectively. By properly fitting, an equivalent circuit of parallel resistor (R_f) and capacitor (C_f) is presented in Fig. 6f. Due to the low water content at low RH, the impedance is dominated by a C_f value since the protons are transported primarily by hopping through the sulfonated groups. With increasing of RH (75%–95% RH), each curve is composed by a semicircle in the high frequency range and a straight line in the low frequency range. In this case, the straight line represents the

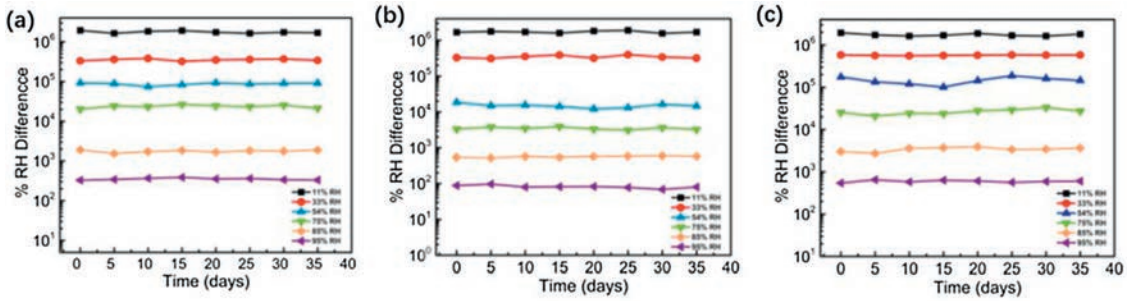

(d)

humidity sensor	maximal fluctuation value	Average fluctuation vales					
		11% RH	33% RH	54% RH	75% RH	85% RH	95% RH
S-4	-5.4%, 30th day at 95% RH	-0.7%	0.5%	-0.6%	1.7%	-1.2%	1.3%
S-6	-2.9%, 5th day at 85% RH	0.1%	0.4%	-2.6%	0.5%	0.7%	-1.9%
S-8	-4.6%, 15th day at 54% RH	-0.8%	-0.1%	-1.9%	0.4%	1.7%	1.7%

Fig. 5. Long-term stability of POSS-PMMA-SPS humidity sensor with different sulfonation degree (a: S-4; b: S-6; c: S-8; d: comparison of impedance fluctuation of three humidity sensors under different RH).

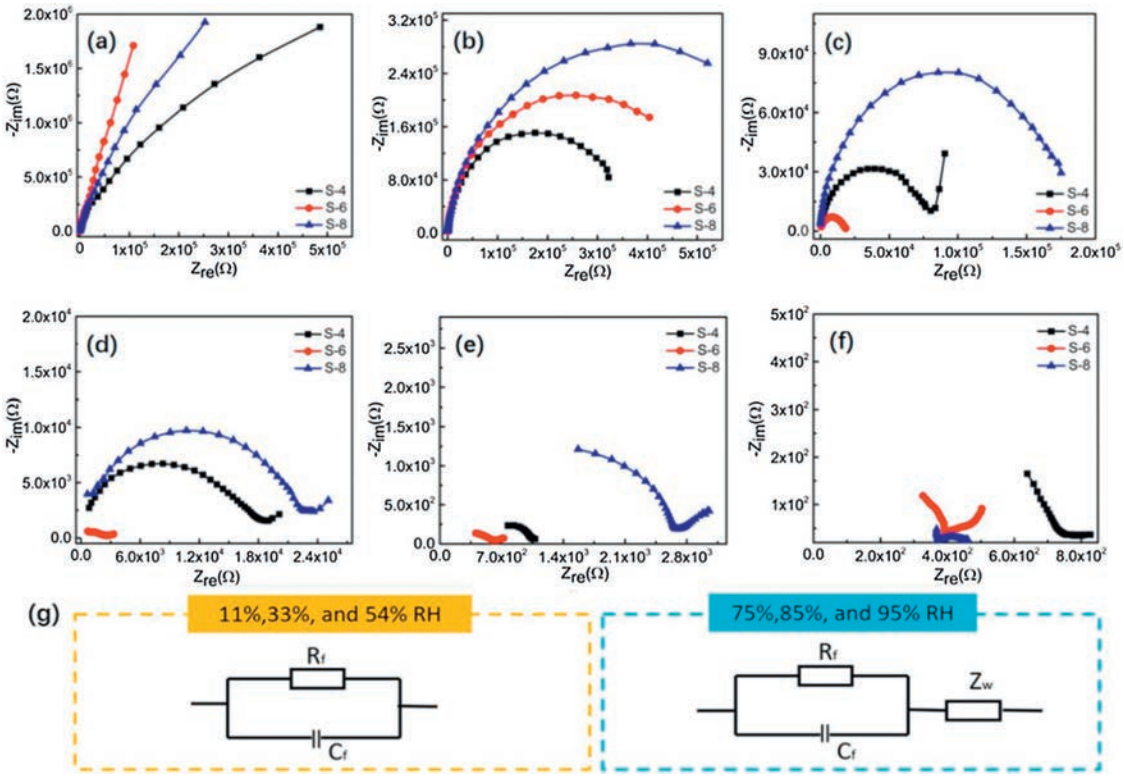

Fig. 6. Nyquist curves and equivalent circuits (EC) model of POSS-PMMA-SPS humidity sensor with different degree of sulfonation: (a) 11% RH, (b) 33% RH, (c) 54% RH, (d) 54% RH, (e) 85% RH, (f) 95% RH; (g) EC models of humidity sensor under different RH.

Warburg impedance and is caused by the contribution from diffusion of electroactive species at the electrode/sensing film interface [3]. In the high RH range, many water molecules are adsorbed on the polymer's surface, leading to formation of water clusters. And the equivalent circuit could be interpreted by R_f and C_f in parallel and then Z_w in series.

In conclusion, a series of tadpole shaped sulfonated POSS containing block polymers (POSS-PMMA-SPS) were synthesized via two-step ATRP followed by post sulfonation for different sulfonation degree. A similar degree of water adsorption over a wide range of RH was found in three BCPs materials (S-4, S-6 and S-8). All three humidity sensors exhibited an impedance change of more than four order of magnitude over a wide range of humidity. The POSS-PMMA–SPS (S-6) sensor exhibited a relatively fast response ($t_{90\%}$ of 11 s and 80 s for adsorption and desorption processes, respectively), and superior repeatability for over 30 days. The moderate degree of sulfonation of the BCPs is a crucial issue for achieving excellent humidity sensing due to a good balance between water adsorption and water interaction with the polymer matrix. This reported study presents a novel molecular architecture of tadpole-shaped POSS-PMMA-SPS and demonstrates its great potential for application in humidity sensor applications.

Declaration of competing interest

The authors declare that they have no known competing financial interests or personal relationships that could have appeared to influence the work reported in this paper.

Acknowledgments

This work is supported by Natural Science and Technology Agency of Shaanxi Province (No. 2019KW-024) and fundamental research funds for the central universities (No. 310201911fz050), and the Open Fund for Key Lab of Guangdong High Property and Functional Macromolecular Materials (No. 20190015).

Appendix A. Supplementary data

Supplementary material related to this article can be found, in the online version, at doi:https://doi.org/10.1016/j.cclet.2020.01.020.

References

[1] Q.N. Zhao, Z. Yuan, Z.H. Duan, et al., Sens. Actuator. B: Chem. 289 (2019) 182–185.
[2] Y. Zhang, Z.H. Duan, H.F. Zou, M. Ma, Sens. Actuator. B: Chem. 261 (2018) 345–353.
[3] Z.H. Duan, M. Xu, T.S. Li, Y. Zhang, H.F. Zou, Sens. Actuator. B: Chem. 258 (2018) 527–534.
[4] Z.H. Duan, Y.D. Jiang, M.G. Yan, et al., ACS Appl. Mater. Interfaces 11 (2019) 21840–21849.
[5] E. Traversa, Sens. Actuator. B: Chem. 23 (1995) 135–156.
[6] S.P. Yawale, S.S. Yawale, A.T. Lamdhade, Sens. Actuator. A: Phys. 135 (2007) 388–393.
[7] W.Y. Xie, B. Liu, S.H. Xiao, et al., Sens. Actuator. B: Chem. 215 (2015) 125–132.
[8] P.G. Su, C.F. Chiou, Sens. Actuator. B: Chem. 200 (2014) 9–18.
[9] Y. Sakai, Y. Sadaoka, M. Matsuguchi, Sens. Actuator. B: Chem. 35 (1996) 85–90.
[10] Y. Sakai, M. Matsuguchi, T. Hurukawa, Sens. Actuator. B: Chem. 66 (2000) 135–138.
[11] T. Fei, H.R. Zhao, K. Jiang, T. Zhang, Sens. Actuator. B: Chem. 208 (2015) 277–282.
[12] D.Z. Zhang, J. Tong, B.K. Xia, Sens. Actuator. B: Chem. 197 (2014) 66–72.
[13] Y. Li, T.T. Wu, M.J. Yang, Sens. Actuator. B: Chem. 203 (2014) 63–70.
[14] Y. Li, C. Deng, M.J. Yang, Sens. Actuator. B: Chem. 194 (2014) 51–58.
[15] C.W. Lee, H.S. Park, J.G. Kim, et al., Sens. Actuator. B: Chem. 109 (2005) 315–322.
[16] D.Z. Zhan, Y.E. Sun, P. Li, Y. Zhang, ACS Appl. Mater. Interfaces 8 (2016) 14142–14149.
[17] K. Jiang, H.R. Zhao, T. Fei, H.M. Dou, T. Zhang, Sens. Actuator. B: Chem. 222 (2016) 440–446.
[18] T. Fei, J.X. Dai, K. Jiang, H.R. Zhao, T. Zhang, Sens. Actuator. B: Chem. 227 (2016) 649–654.

[19] Y. Li, Y.S. Chen, C. Zhang, T.X. Xue, M.J. Yang, Sens. Actuator. B: Chem. 125 (2007) 131–137.
[20] Y. Li, K.C. Fan, H.T. Ban, M.J. Yang, Sens. Actuator. B: Chem. 222 (2016) 151–158.
[21] N.W. Li, M.D. Guiver, Macromolecules 47 (2014) 2175–2198.
[22] B. Bae, T. Yoda, K. Miyatake, H. Uchida, M. Watanabe, Angew. Chem. Int. Ed. 49 (2010) 317–320.
[23] J. Zhang, F. Chen, X.Y. Ma, et al., Int. J. Hydrogen Energy 40 (2015) 7135–7143.
[24] W.C. Geng, X.W. He, Y.W. Su, et al., Sens. Actuator. B: Chem. 226 (2016) 471–477.
[25] E. Kim, S.Y. Kim, G. Jo, S. Kim, M.J. Park, ACS Appl. Mater. Interfaces 4 (2012) 5179–5187.
[26] Y. Li, H.J. Zhao, M.F. Jiao, M.J. Yang, Sens. Actuator. B: Chem. 257 (2018) 1118–1127.
[27] J.X. Dai, T. Zhang, H.R. Zhao, T. Fei, Sens. Actuator. B: Chem. 242 (2017) 1108–1114.
[28] F. Chen, F. Lin, Q. Zhang, et al., Macromol. Rapid Commun. (2019)1900101.
[29] J.C. Yang, M.J. Jablonsky, J.W. Mays, Polymer 43 (2002) 5125–5132.
[30] G.W. He, Z. Li, J. Zhao, et al., Adv. Mater. 27 (2015) 5280–5295.
[31] Z. Zhuang, Y.F. Li, D. Qi, C.J. Zhao, H. Na, Sens. Actuator. B: Chem. 242 (2017) 801–809.